HHS Public Access

Author manuscript

Nat Struct Mol Biol. Author manuscript; available in PMC 2011 December 01.

Published in final edited form as:

Nat Struct Mol Biol. 2011 June ; 18(6): 701–707. doi:10.1038/nsmb.2058.

Structure of the ATP synthase catalytic complex (F_1) from *Escherichia coli* in an auto-inhibited conformation

Gino Cingolani[1] and **Thomas M. Duncan**[2]

[1] Department of Biochemistry and Molecular Biology, Thomas Jefferson University, Philadelphia, PA 19107, USA

[2] Department of Biochemistry and Molecular Biology, SUNY Upstate Medical University, Syracuse, NY 13210, USA

Abstract

ATP synthase is a membrane-bound, rotary motor enzyme that is critical for cellular energy metabolism in all kingdoms of life. Despite conservation of its basic structure and function, auto-inhibition by one of its rotary stalk subunits occurs in bacteria and chloroplasts but not in mitochondria. The crystal structure of the ATP synthase catalytic complex (F_1) from *Escherichia coli* described here reveals the structural basis for this inhibition. The C-terminal domain of subunit ε adopts a novel, highly extended conformation that inserts deeply into the central cavity of the enzyme and engages both rotor and stator subunits in extensive contacts that are incompatible with functional rotation. As a result, the three catalytic subunits are stabilized in a set of conformations and rotational positions distinct from previous F_1 structures.

INTRODUCTION

Adenosine triphosphate (ATP) is a key energy carrier in cellular metabolism. Most ATP is synthesized during oxidative- or photo-phosphorylation by the proton-translocating ATP synthase (F_OF_1-ATPase). This energy-transducing enzyme functions as a rotary motor and is conserved from bacteria to mitochondria and chloroplasts. A proton-motive force (PMF) is generated across a membrane during respiration or photosynthesis, and this PMF drives the transport of protons (Na^+ in some bacteria) through the membrane-embedded F_O complex of the ATP synthase. F_O is connected by a peripheral stator and a central rotor to the extrinsic F_1 complex, which contains the catalytic sites for ATP synthesis. Proton transport at the

Correspondence should be addressed to G.C. (gino.cingolani@jefferson.edu) or T.M.D. (duncant@upstate.edu).

AUTHOR CONTRIBUTIONS

T.M.D. developed a purification protocol to obtain homogeneous EF_1-δ. T.M.D. and G.C. crystallized EF_1-δ. G.C. collected X-ray data and determined the crystal structure. T.M.D. wrote the manuscript with the help of G.C.

COMPETING INTERESTS STATMENT

The authors declare no competing financial interests.

Accession codes

Structure factors and atomic coordinates for the EF_1 structure were deposited in the Protein Data Bank with accession code 3OAA.

Note: Supplementary information is available on the Nature Structural & Molecular Biology website.

rotor stator interface in F_O drives turbine-like rotation of the rotor's ***c***-ring, which directly couples to the rotor subunits of F_1. Subunit γ forms the main, asymmetric shaft of F_1's rotor, and transport-driven rotation of γ relative to the surrounding $\alpha_3\beta_3$ complex of F_1 drives alternating conformational changes in the three catalytic β subunits to drive net synthesis of ATP[1–3]. Rotational coupling is reversible and, if PMF drops below the energetic threshold needed to drive ATP synthesis, net ATP hydrolysis by the alternating catalytic sites on F_1 can drive reverse rotation of γ and the ***c***–ring of F_O, thus pumping protons across the membrane in the opposite direction. *In vitro*, F_1 can be dissociated from membranes as a soluble ATPase, and crystal structures of mitochondrial F_1 (MF_1) have provided invaluable insights on the enzyme's architecture and rotary mechanism[4–7]. However, few structural details are available for bacterial F_1-ATPases[8–10], which have been exploited extensively for mechanistic studies[2,3].

The other subunit of F_1's rotor shaft is ε (δ in MF_1). In all types of ATP synthase, ε's N-terminal domain (NTD) binds to γ and directly couples to the ***c***–ring of F_O. In bacteria and in chloroplasts, ε's C-terminal domain (CTD) is thought to function as a mobile regulatory element that can change conformation in response to nucleotide conditions and/or PMF[2,11,12]. Growing evidence indicates that inhibition by εCTD involves direct contacts with catalytic β subunit(s). For instance, residues εS108 and βE381 of the *Escherichia coli* enzyme can be readily cross-linked *in vitro* and this interaction is modulated by nucleotide conditions. Meanwhile, there is no evidence for a regulatory role by the homolog of ε in mitochondrial ATP synthases, and residues analogous to *E. coli*βE381 and εS108 are more than 50 A apart in the structure of MF_1[13]. Furthermore, in MF_1 a unique mitochondrial subunit (known as ε_M) stabilizes ε's homolog in a compact conformation that makes no direct contacts with $\alpha_3\beta_3$. Finally, a distinct inhibitor protein has evolved for regulation of the mitochondrial enzyme[14]. Thus, there appear to be significant differences both in the composition of the rotor shaft and in regulation of catalytic activity of bacterial ATP synthases as compared to their mitochondrial homolog.

To provide an atomic description of a prototypical bacterial F_1, we have determined the first high-resolution crystal structure of the ATP synthase catalytic complex (F_1) from *Escherichia coli* in an auto-inhibited conformation. The structure provides a clear view of ε's inhibitory conformation within the F_1 complex and thereby sheds light on a regulatory feature that is unique to ATP synthases of bacteria and chloroplasts. Furthermore, bacterial ATP synthase, and not its mitochondrial counterpart, is the proven target for a recently discovered type of anti-tuberculosis drug[15]. Thus the structure for ε-inhibited F_1 of *E. coli* ATP synthase will be particularly valuable for developing new antimicrobials that target bacterial but not mitochondrial ATP synthases.

RESULTS

Structure Determination and Overall Architecture of EF_1

Crystallization studies of *E. coli* F_1 (EF_1) began nearly two decades ago, but progress was hindered by the limited homogeneity of purified samples of this multi-subunit enzyme that contains nine polypeptide chains (composition: $\alpha_3\beta_3\gamma\delta\varepsilon$). Thus far, only a low-resolution, main chain model of EF_1 depleted of the peripheral stator subunit δ has been reported[8].

Aiming for a high-resolution structure, we used high-throughput crystallization screening of EF_1 depleted of subunit δ (henceforth called EF_1) and identified a distinct crystal form that contains four EF_1 complexes in the asymmetric unit (M.W. ~1.5 MDa). The diffraction quality of EF_1 crystals was gradually improved by controlled dehydration in the presence of nucleotide. Complete diffraction data to 3.26 Å resolution were measured at the National Synchrotron Light Source (NSLS), beamline X25. A complete atomic model was built in a 4-fold averaged electron density map and refined to R_{work}/R_{free} ~24.3/26.4% at 3.26 Å resolution (Table 1, Supplementary Fig. 1). Sequence registers for all eight chains ($\alpha_3\beta_3\gamma\varepsilon$) were confirmed using the anomalous signal of 89 selenium peaks. The general architecture of EF_1 is analogous to that of MF_1 and is illustrated in Figure 1a,b. A hexamer of alternating α- and β-subunits surround the upper region of the central rotor stalk, which consists of an antiparallel coiled-coil of the N- and C-terminal α-helices of γ (γNTH–γCTH, Fig. 1c). Nucleotide binding sites on β subunits are responsible for ATP synthesis and hydrolysis, while sites on α subunits are noncatalytic. In the $\alpha_3\beta_3$ hexamer, the catalytic site of each β is at an interface with a specific α. Based on conserved β-γ interactions, the numbered β subunits correspond to MF_1 nomenclature[4] with $\beta1 = \beta_{DP}$,$\beta2 = \beta_E$, $\beta3 = \beta_{TP}$. Each of the three α subunits has a noncatalytic site with clear density for bound Mg·ATP or Mg·AMPPNP, although α3 has lower occupancy (Supplementary Fig. 2). Only one specific β subunit, β1, has nucleotide bound at its catalytic site (Fig. 1, Supplementary Fig. 2).

Below the $\alpha_3\beta_3$ 'head', γ's coiled-coil protrudes ~45 Å and is flanked on one side by γ's globular Rossmann-fold domain, and on the other by the εNTD. In all ATP synthases, it is the base of γ and the εNTD that connect to the rotary ***c***-ring of F_O (Fig. 1a), and the εNTD is essential for functional coupling of F_1 to F_O[2]. Both γ and ε are exceptionally well resolved in the EF_1 structure, and the εCTD is the most unique feature (Figs. 1, 2). It adopts a highly extended state (denoted ε_X) that contacts five of the seven other subunits, including both domains of γ and the CTDs of α1, α2, β1 and β3, and the last half of the εCTD inserts deeply into the central rotor cavity (Fig. 1a,b). This contrasts with ε's homolog in MF_1 structures, in which the εCTD is far from $\alpha_3\beta_3$ and folded compactly against the εNTD[13]. A similar compact state (denoted ε_C) is observed for isolated bacterial ε[16–18], and bacterial F_OF_1 retains coupled functions with ε trapped in the ε_C state[19]. Superimposing εNTD of ε_C and ε_X states reveals striking differences in the fold of the εCTD (Fig. 2). The final β-strand of the εNTD in ε_C (Fig. 2c, β-strand10) is unfolded in ε_X, forming a loop that begins the εCTD in EF_1 (Fig. 2b, loop1). Following εloop1, εhelix1 starts and ends earlier in ε_X, so that εloop2 is longer (ε103–111; Fig. 2c *vs.* 2b) than in the ε_C state. In contrast, εhelix2 is shorter in ε_X (ε112–125) and the terminal segment, which we name the εhook (ε126–138), bends sharply away (73° crossing angle, εhelix2 *vs.* helix of εhook). The regions of εCTD that contact β1 and β3 in EF_1 agree with previous chemical labeling and cross-linking studies[17]. Most telling, direct ε–β cross-linking[20] showed close contact for εSer108 and βGlu381 of β1 (Fig. 1b), and these sidechains are within hydrogen bonding distance in the EF_1 structure (Fig. 3a). Proximity of εSer108 to βGlu381 (on any β) cannot be explained by the ε_C state (Fig. 2a) or by a distinct extended state of *E. coli*ε seen in a complex of ε with only a truncated γ[21] (γ′–ε, Supplementary Fig. 3). Thus, only the ε_X conformation reported here in EF_1 is consistent with biochemical data for ε–β inhibitory interactions.

Interactions of εCTD with Other EF_1 Subunits

The εCTD has three regions of contact with other EF_1 subunits (Fig. 2b). In region 1, ε's loop1 and helix1 contact only γ (Figs. 1a, 2a); εloop1 forms a salt bridge with the γCTH (εArg85–γGlu224) and εhelix1 packs mainly against γ's Rossmann-fold. In region 2 (Fig. 3a), εloop2 and εhelix2 contact five other chains (α1, α2,β1, β3, γ), with εhelix2 inserted into the central rotor cavity. εhelix2 and γNTH form an antiparallel coiled-coil, with substantial burial of hydrophobic residues, that is also stabilized by hydrogen bonds at both ends and by electrostatic contacts (γArg84, γLys30 with εAsp111). The position of εhelix2 between β1's CTD and γ blocks specific β1–γ interactions that are seen in MF_1 structures and thought to be important for rotational coupling[5,7,13]. The CTDs of α1 and α2 also contact εhelix2 from either side (Fig. 1b), apparently helping clamp εhelix2 in position (Fig. 3a). Contact region 3 spans the εhook (ε126–138), which contacts γNTH, γCTH and wraps partly around helix1 of β3's CTD (Fig. 3b). The εhook also contacts β3 near βTyr331, a part of the adenine-binding pocket. In comparison, region 2 involves more specific bonds of εloop1 and helix2 with other subunits, but much more contact surface is buried in region 3 between β3 and εhook than between β1 and ε in region 2. Overall, contacts of εCTD with other subunits bury ~2900 $Å^2$ of surface area and ~70% of this involves the segment of εCTD inserted within the central rotor cavity (ε109–138). Of the surface buried by ε109–138, ~56% is with α and β subunits. These extensive rotor–stator interactions are expected to prohibit rotation of γε relative to $\alpha_3\beta_3$ when ε adopts the ε_X state. This agrees with a recent study of forced rotation of thermophilic bacterial F_1 in which activation from an ε-inhibited state required much greater rotary torque than activation from an ADP-inhibited state[22]. Thus, the ε_X state observed crystallographically in EF_1 correlates with the ε-inhibited state that blocks both hydrolysis and synthesis of ATP by EF_OF_1[23].

Distinct Features of Catalytic β subunits

EF_1 is the first F_1 structure determined in which only 1 of 3 catalytic sites has bound nucleotide (Fig. 1a,b, Supplementary Fig. 2), and the catalytic β subunits show a combination of conformational states not seen before (Fig. 4). Most MF_1 structures are similar to the 1.9 Å ground-state of MF_1[5]: β1 and β3 are each in a 'closed' state with bound nucleotide, but β2 has an open state without nucleotide, since contacts of its CTD with a convex surface of γ distort the nucleotide binding site[4]. In EF_1, β2 adopts the usual open state and makes no contacts with the εCTD. β3 adopts the basic closed state but has no bound nucleotide, although its interface with the εhook causes minimal distortions relative to β3 of MF_1. However, β2 and β3 each have SO_4^{2-} bound at the P-loop (Supplementary Fig. 2), in a position nearly identical to that occupied by PO_4^{2-} on β3 of nucleotide-free yeast MF_1[24]. Finally, β1 cannot assume the usual closed state, due to insertion of εhelix2 between β1's CTD and γ. β1 is also not in the open state, but adopts a half-closed state with bound ADP and SO_4^{2-}. A unique MF_1 structure, with nucleotide bound on all three β (denoted here as MF_1-3filled), has one β in the same half-closed state (Fig. 4c) with bound ADP and SO_4^{2-}, but at the β2 position that is typically in the open state[7]. The positions of bound Mg·ADP, SO_4^{2-} and key ligand-binding residues also align closely between β2 of MF_1-3filled and β1 of EF_1 (Fig. 4d). Thus, the εCTD does not distort β1 into a unique state, but traps it in an intermediate conformation that was seen before, but in a different rotary position of β relative to γ.

Correlations with Functional Rotary Mechanics

The surprising finding of a half-closed conformation of β1 in EF_1 prompted us to compare the rotary arrangement of the three catalytic sites around γ in EF_1 to that of MF_1 structures. Single-molecule studies have shown that each 120° rotation (associated with net hydrolysis of one ATP) involves two sequential kinetic substeps: ~80° rotation follows ATP binding at one catalytic site, and ~40° rotation follows the catalytic pause limited by hydrolysis and release of product(s) at an alternate site[25,26]. Thus far, most MF_1 structures were thought to exhibit one orientation of $\alpha_3\beta_3$ around γ, but significantly different rotary positions were noted for MF_1(3-filled)[7] and for one conformation of yeast MF_1 (yF_1I)[27]. It was suggested that MF_1(3-filled) represents the catalytic dwell position (before the 40° step) and that yF_1I represents the ATP binding position (before the 80° step)[28]. As a new approach to align F_1 structures and compare their relative rotary positions, we identified a structural core of γ that has minimal deviations between different F_1 structures (Supplementary Figs. 4, 5; Supplementary Methods). A stiff γ-core structure is considered necessary to drive alternating conformational changes in the β subunits during rotation; the γ-core identified here overlaps with stiff regions indicated by single-molecule studies with EF_1[29] and includes most γ residues noted for torque generation in molecular dynamics studies with MF_1[28]. The γ-core includes significant portions of γ's coiled-coil and Rossmann-fold domains (Supplementary Fig. 5), and so provides a robust reference for superimposing F_1 structures and comparing rotary positions of the three catalytic sites around γ (Supplementary Fig. 6). Figure 5a illustrates that the β subunits of MF_1(3-filled) are rotated farthest in the direction of net ATP synthesis, as noted before, whereas those of EF_1 are rotated farthest in the direction of ATP hydrolysis. The distinct rotary position of ε-inhibited EF_1 is supported by electron microscopy studies of EF_1[30] and by single-molecule fluorescence studies of EF_OF_1-liposomes[31]. The 43° rotary shift from MF_1(3-filled) to EF_1 correlates with the 40° step following the catalytic dwell, and rotating EF_1 farther by 78° would superimpose its half-closed β1 with the half-closed β2 of MF_1(3-filled). Thus, the ε_X state appears to trap EF_1 in a rotary position close to the kinetic dwell before the next ATP binding event and 80° rotary step. Bound product(s) on the half-closed β before (EF_1, β1) and after the 80° step (MF_1(3-filled), β2) support the linkage of product dissociation to the 40° step and the original contention that MF_1(3-filled) represents the rotary state post-hydrolysis but prior to product release from its half-closed β2[7].

Aligning F_1 structures by their shared γ-core provides additional visual clues to the complex movement of β subunits relative to γ during functional rotation, which was suggested by normal-mode analysis[32]. This is illustrated in side views showing just the distinct positions of β2 (Fig. 5b) and β3 (Fig. 5c) for γ-aligned structures that span the 40° rotary step. The 80° rotary step has a central axis parallel to γ's vertical shaft (red line, Fig. 5b,c), but the different positions of each β along the 40° step suggest a more complex pivoting around γ's asymmetric features. Also, specific β-γ contacts or "catches"[4] may restrict the distinct pivoting of β2 *vs*β3 across the 40° step, as hydrogen bonds of catch-1 (β2-γ, Fig. 5b) and catch-2 (β3-γ, Fig. 5c) are maintained through the range of rotary states shown. Thus, the three states of β2 remain close in the upper region near catch-1 but are farther apart at the base, whereas the β3 states are close at the base near catch-2 but farther apart in the upper region; positions of β1 around γ in different structures indicate β1 does not pivot much

during the 40° step (not shown). The different pivoting of β2 *vs*β3 should also correlate with opening or closing of the different α–β catalytic interfaces during rotation, which is thought to be important in modulating the functional states of the alternating sites[4]. Finally, γ-core alignment of F_1 structures suggests that, during the 40° rotary step, the final segment of the γCTH (~20 residues) is bent in different directions (Supplementary Fig. 5b) by the "hydrophobic sleeve" region of $\alpha_3\beta_3$ that surrounds it[4]. Flexibility of this final segment of γCTH is consistent with results of single-molecule studies and molecular dynamics simulations[33]. The direction of the γCTH bend correlates with F_1's rotary position being <20° (Supplementary Fig. 5b, circled) or >20° in the direction of ATP hydrolysis. This correlation holds true for all MF_1 structures aligned by γ-core (not shown) with one exception (see Supplementary Fig. 6). Accordingly, the correlation between the γCTH bend and F_1's rotary position could suggest a rotary transition point at which torque between γ and $\alpha_3\beta_3$ is sufficient to induce a distinct bend in the final segment of γCTH.

DISCUSSIONS

Physiological regulation of ATP synthases

The structure described in this paper reveals the first molecular view of the ε-inhibited state that can occur in ATP synthases in most bacteria and in chloroplasts: the εCTD adopts a highly extended conformation (ε_X) that partly inserts into the central rotor cavity, bridging between γ's rotary stalk and surrounding catalytic subunits to prevent functional subunit rotation (Fig. 6a,c). This structural snapshot of the εCTD within *E. coli* F_1 agrees with a wealth of cross-linking and functional data on ε's inhibitory interactions with bacterial ATP synthases, so far not explained by structures of eukaryotic F_1. In contrast, the mitochondrial homolog of ε is believed to be non-inhibitory, with its CTD clamped in the compact ε_C state by a unique mitochondrial subunit (Fig. 6d,f)[13]. Instead, eukaryotes evolved a separate protein, IF_1, to inhibit mitochondrial ATP synthase[14]. Nevertheless, these distinct inhibitor proteins serve the same primary role, to block 'wasteful' ATP hydrolysis by F_OF_1 under conditions when the PMF across the membrane is low or absent. In mitochondria, respiration and PMF decline dramatically during cellular hypoxia, which occurs for instance during cardiac failure. Without PMF to drive ATP synthesis, F_OF_1 begins to work in reverse, but acidification of the mitochondrial matrix transforms IF_1 into an active form that binds to and inhibits MF_1, minimizing wasteful ATP hydrolysis and the odds of cell death. In plants, chloroplasts regularly lose PMF during long dark cycles, and inhibition by ε coordinates with a chloroplast-specific adaptation of γ to inactivate the ATP synthase in the dark[12]. Bacteria are more varied in their environmental and metabolic demands, and the physiological role of ε inhibition may be tuned to these differences in bacterial ecology; this is consistent with the variations in sequence and length of εhelix2 between different types of bacteria[11] and with the fact that some aerobic bacteria exhibit much stronger ε-inhibition on membranes than observed with *E. coli*[34]. Some bacteria can neither respire nor photosynthesize, but require their F_OF_1 to function as an ATPase-driven proton pump in order to maintain PMF and/or internal pH homeostasis[35]. Moreover, while facultative anaerobes such as *E. coli* can respire, they also need F_OF_1 to function as an ATPase-driven proton pump in anaerobic conditions, which can occur along the digestive tract of their hosts. Thus, similar to previous arguments[36], bacterial ε is not generally geared to inhibit

F_OF_1 whenever thermodynamics favor ATP hydrolysis, but rather inhibits ATPase-driven proton pumping when it is wasted by failing to generate substantial PMF across the cell membrane. In *E. coli*, for instance, this can occur when high concentrations of membrane-permeant acids arise from fermentation or from their host's digestive processes, and it is known that F_OF_1 is important for one acid-resistance mechanism of *E. coli*[37]. Nevertheless, further studies will be needed to determine specific environmental conditions where autoinhibition by ε subunit confers a selective advantage for growth or survival of different bacteria.

Comparisons of ATP synthase inhibitor proteins

Despite the distinct origins of the bacterial inhibitor εCTD and the mitochondrial inhibitor IF_1, there are broad similarities in the way these two endogenous inhibitors interact with the F_1 catalytic core (Fig. 6). In each case, the inhibitory segment is mainly α-helical, is inserted at the α1–β1 catalytic interface, and contacts the same five subunits (α1, α2, β1, β3, γ). Each inhibitory region buries extensive surface area (ε106–138, ~2100 Å^2; IF_1, ~2700 Å^2) and has specific interactions buried deeply within F_1. It was proposed that IF_1 inserts at a prior rotary position, with a more open α–β interface, and then is buried by subsequent rotation and conformational changes in MF_1[6]. With EF_OF_1, ε's conformational change is blocked by preventing rotation of the ***c***–ring in F_O[38], suggesting at least a rotary substep is linked to ε's transition to or from the inhibited state. Rotational entrapment may also correlate with the bent shape of each inhibitor's most buried end, although εCTD and IF_1 are bent in different directions (Fig. 6a *vs.* 6d); in the isolated γ′–ε complex[21], εhelix2 is long and unbent as in ε_C (Supplementary Fig. 3), suggesting the bent εhook in EF_1 is induced by interactions with $\alpha_3\beta_3$. Reversing inhibition of F_OF_1 also has a common factor. PMF stimulates dissociation of IF_1 to activate MF_OF_1[39], and it was proposed that PMF-driven rotation in the direction of ATP synthesis causes IF_1 to be expelled[6]. PMF activates the latent chloroplast enzyme and causes the εCTD to become exposed[12]. Activation by PMF also occurs with ATP synthases of bacteria, including *E. coli*[40], and preliminary evidence links this to relief of inhibition by εCTD[41]. Thus, whereas most bacteria retain *in cis* auto-inhibition by the εCTD, eukaryotes have evolved IF_1 for a similar mode of inhibition, although it acts *in trans*.

Model for the regulatory transition between the ε_C and ε_X conformations

We propose a basic series of molecular events for the transition between the ε_C and ε_X states in bacterial ATP synthase, as summarized in Figure 7. An early step from ε_C to ε_X should be to disrupt the interface of εhelix2 with the εNTD, and several mutations in εNTD that alter inhibition are near εhelix2 in the ε_C state[42]. For some bacteria, the ε_C state can be stabilized by binding of ATP to a low-affinity site that bridges the εhelix2–εNTD interface, thus favoring active complexes when cellular ATP is abundant[18]. We speculate that the stability of the εhelix2–εNTD interface could also be influenced by the transmission of rotary torque between γ–εNTD and the ***c***–ring of F_O; the apparent torsional compliance of the bottom regions of γ–εNTD[29], which interface with the ***c***—ring, could distort the εhelix2–εNTD interface when PMF induces torque through the ***c***–ring. Another possibility is that εhelix2–εNTD and/or εhelix1–helix2 interactions in ε_C may be directly influenced by the membrane potential component of PMF; εhelix1 and helix2 lie close and nearly parallel to the plane of the membrane in the ε_C state and contain many charged residues. Separation of εhelix1 from

εhelix2 should also occur early, since the face of εhelix1 that contacts εhelix2 in ε_C instead interacts with γ in the ε_X state. We propose that a kinetically appreciable intermediate state of ε then forms by docking of εhelix1 to γ, as in ε_X, but with εhelix2 exposed and mobile below $\alpha_3\beta_3$ (Fig. 7, center). This is supported by proteolysis studies in which cleavage of ε initiates in εhelix2[17,38]. Trypsin cleavage is slow for isolated ε (ε_C state) and for EF_OF_1 in the presence of MgADP and Pi, which favors the ε_X state; this is consistent with limited exposure of εhelix2 in the ε_C state (packed between εhelix1 and the εNTD) and in the ε_X state (buried within EF_1's central cavity). Trypsinolysis of ε in EF_OF_1 is much faster in the presence of MgAMPPNP, which may favor ε_C but also favors ε–α cross-linking instead of ε–β cross-linking[43]. Thus an intermediate state as shown, with εhelix1 bound to γ, would keep εS108 of εloop2 near $\alpha_3\beta_3$ but would leave εhelix2 exposed for cleavage by trypsin. This intermediate should enhance the kinetics for insertion of εhelix2 into EF_1's rotor cavity in the next step, when transition of β1 towards the half-closed state and partial rotation of γ create an opening sufficient for εhelix2 to insert and form a coiled-coil with γNTH. Further subunit rotation would then occur, burying εhelix2 within the central cavity and disrupting the end of εhelix2 to form the εhook. Once stabilized with ε in the ε_X state, expelling εhelix2 to return F_OF_1 to an active state would probably require rotary torque from F_O in the direction of ATP synthesis; consistent with this, it was noted earlier that PMF activates bacterial F_OF_1. Further experiments will be needed to elucidate details of this intriguing regulatory mechanism for ATP synthases of bacteria and chloroplasts.

Concluding remarks

Functional ATP synthase is essential for higher organisms, but is also critical for the viability of pathogenic bacteria such as *Streptococcus pneumoniae*[44] and *Mycobacterium tuberculosis*[45]. Even enterohemorrhagic *E. coli* cannot compete for an intestinal niche if it lacks the ATP synthase[46]. Differences in structural complexity and regulation between bacterial and mitochondrial ATP synthases can be exploited to selectively inhibit the former. The structure of ε-inhibited EF_1 presented in this paper provides a rational framework for developing antimicrobial agents that selectively mimic or stabilize the ε-inhibited state but do not inhibit mitochondrial ATP synthase.

METHODS

Protein expression and purification

EF_OF_1 was expressed from plasmid pJW1[48] in *E. coli* strain JP17[49]. Cell were grown and membranes isolated as described[48]. To incorporate selenomethionine (SeMet) into EF_OF_1, pJW1 was expressed in *metB*$^-$ strain LE392Δ(atpI–C)[50]; cells from rich-medium starter cultures were collected by centrifugation, washed with defined medium without methionine[51], then grown in 10 L of the same medium with 0.1 g of SeMet per liter. EF_1 was purified as before[52], but the ion exchange step used 50 ml of Macro-Prep High Q resin (Bio-Rad) and a linear gradient from 0 to 350 mM NaCl (250 ml at 2 ml min^{-1}). EF_1 was depleted of subunit δ by gel filtration[8] (Sephacryl S-300, HiPrep 16/60, GE Life Sciences) at 22°C in the presence of 0.2% (w/v) lauryldimethylamine oxide; δ-depleted EF_1 was dialyzed extensively (10 kDa MWCO) against column buffer without detergent, concentrated to >15 mg ml^{-1}, frozen in liquid N_2 and stored at −80°C.

Crystallization and X-ray data collection

Before crystallization, δ-depleted EF_1 (or SeMet-substituted EF_1, SeMet-EF_1) was dialyzed at ~5 mg ml^{-1} *vs.* TE75 buffer (50 mM Tris-HCl, 0.1 mM Na_2EDTA, pH 7.5) for 12–18 hr at room temperature (RT), including one buffer change, then concentrated by ultrafiltration to ≥20 mg ml^{-1}. At this point, EF_1 retained endogenous adenine nucleotides (mol per mol EF_1: total, 2.74 ±0.16; noncatalytic, 1.03 ±0.23 ADP, 0.68 ±0.1 ATP; catalytic, 0.97 ±0.09 ADP, <0.12 ATP). EF_1 and SeMet-EF_1 were crystallized at RT by hanging-drop vapor diffusion. EF_1 at 20 mg/ml (typically 3 μl) was mixed with an equal volume of 0.1 M MOPS-NaOH, pH 7, 75–150 mM $MgSO_4$, 7–9% (w/v) PEG8000, 5 mM β-mercaptoethanol and equilibrated against 600 μl of the same solution. Crystals were screened for diffraction at NSLS beamlines X6A and X25 as well as macCHESS stations A1 and F1. Diffraction quality was improved by controlled dehydration in solutions containing 25% (v/v) glycerol, in the presence of 1 mM AMPPNP. A complete dataset to a resolution limit of ~3.26 Å was obtained at NSLS beamline X25 (Table 1). A 5.0 A dataset for a SeMet-EF_1 crystal was collected at NSLS beamline X6A at the selenium edge (~0.972 Å) (Table 1). All data were processed and scaled in HKL-2000[53]. EF_1 crystals belong to space group C2 with four EF_1 complexes in the asymmetric unit.

Structure determination and refinement

The structure of EF_1 was solved by molecular replacement with PHASER[54], using $\alpha_3\beta_3$ of an MF_1 structure (PDB entry 2CK3[55]) as search model. Initial phases were dramatically improved by iterative cycles of solvent flattening, histogram matching, and 4-fold non-crystallographic symmetry averaging with DM[56]. A 4-fold averaged map revealed striking electron density features for the γ and ε subunits, which were not present in the initial phasing model. The averaged 3.26 Å map allowed straightforward interpretation of most side chains. Anomalous scattering peaks from the SeMet-EF_1 dataset helped confirm the register of each chain in EF_1. An atomic model containing all 8 chains in EF_1 ($\alpha_3\beta_3\gamma\varepsilon$) was manually built in Coot[57] and refined with PHENIX[58]. Finally, complete atomic models were built for all four EF_1 complexes in the asymmetric unit (referred to as EF_1-1, EF_1-2, EF_1-3, EF_1-4). Complexes EF_1-1 (chains A H) and EF_1-2 (chains I–P) have better-defined electron densities than EF1-3 (chains Q–X) and EF_1-4 (chains Y, Z, a–f). For all structural analyses and illustrations described in this study, complex EF_1-1 was used as reference. The pairs of α and β subunits that form the three distinct catalytic interfaces in EF_1 are numbered 1–3 in the main text. For example, with complex EF_1-1, these correspond to chains as follows: α1,β1 = C, D; α2, β2 = A, E; α3, β3 = B, F. In the final deposited model, all four EF_1 complexes in the asymmetric unit include residues 25–511 of α1 (chains: C; K; S; a); residues 24–511 of α2 (chains: A; I; Q; Y); residues 26–511 of α3 (chains: B; J; R; Z); residues 2–459 of all β subunits (chains: D, E, F; L, M, N; T, U, V; b, c, d); residues 1–284 of each γ (chains: G; O; W; e) and residues 1–138 of each ε (chains: H; P; X; f). In all α chains, weak density is observed for the solvent-exposed loop 310–318 (residues EAFTKGEVK), which was modeled as poly-alanine in α1 (chains: C; K; S; a) and for residues Leu-448 and Ile-464, which were modeled as alanines in all α chains. Further, in α3 (chains: B; J; R; Z), residues 402–414 have poor density and were partially modeled as poly-alanine between residues 404–408 and 410–416. All β chains in the structure contain the

spontaneous point mutation K81E, which is solvent-exposed and does not affect EF_1 activity[59]. Finally in all γ chains, residues 60–61 have poor density and were modeled as alanines. Ligands bound to EF_1 (Supplementary Fig. 2) include: Mg·ANP on every α chain; Mg·ADP and SO_4^{2-} on the β1 subunit of each complex (chains D, L, T, b); a SO_4^{2-} ion on each β2 chain (E, M, U, c) and on each β3 chain (F, N, V, d). Although a quantitative analysis of ligand occupancy is impossible at this resolution, the Mg·ANP bound to α3 chains (B, J, R, Z) is significantly less occupied than those bound to α1 and α2 chains. Likewise, the SO_4^{2-} ion bound to β2 chains (E, M, U, c) has reduced occupancy as compared to that bound toβ3 chains (F, N, V, d). Additional strong peaks of density (4–6σ above background) were noted in the final Fo–Fc difference map (i) coordinating with ε-Ser65 and (ii) in a pocket inside the γ subunit. Finally, 66 water molecules were modeled in 3.5σ peaks of Fo–Fc density, mainly in proximity to EF_1-1 subunit γ (chain G). The final model was refined to R_{work}/R_{free} ~24.3/26.4% at 3.26 Å resolution (Table 1). Structural figures were prepared with Chimera[60].

Supplementary Material

Refer to Web version on PubMed Central for supplementary material.

Acknowledgments

We dedicate this to the memory of Vladimir Bulygin, Ph.D. (1964–2009), who was instrumental in early stages of the project. We thank Marcus Hutcheon for skillful protein purification. Financial support was provided by the US National Institute of Health (R01GM083088). We thank the staff at NSLS beamlines X6A, X25 (Brookhaven National Laboratory, NY, USA) and at macCHESS (Cornell University, NY, USA) for beam time and assistance in data collection.

References

1. Boyer PD. The ATP synthase--a splendid molecular machine. Annu Rev Biochem. 1997; 66:717–749. [PubMed: 9242922]
2. Duncan, TM. The ATP Synthase: Parts and Properties of a Rotary Motor. In: Hackney, DD.; Tamanoi, F., editors. The Enzymes, vol. XXIII: Energy Coupling and Molecular Motors. Vol. 23. Elsevier Academic Press; New York: 2004. p. 203-275.
3. Junge W, Sielaff H, Engelbrecht S. Torque generation and elastic power transmission in the rotary F_OF_1-ATPase. Nature. 2009; 459:364–70. [PubMed: 19458712]
4. Abrahams JP, Leslie AG, Lutter R, Walker JE. Structure at 2.8 Å resolution of F_1-ATPase from bovine heart mitochondria. Nature. 1994; 370:621–628. [PubMed: 8065448]
5. Bowler MW, Montgomery MG, Leslie AG, Walker JE. Ground state structure of F_1-ATPase from bovine heart mitochondria at 1.9 Å resolution. J Biol Chem. 2007; 282:14238–42. [PubMed: 17350959]
6. Gledhill JR, Montgomery MG, Leslie AG, Walker JE. How the regulatory protein, IF_1, inhibits F_1-ATPase from bovine mitochondria. Proc Natl Acad Sci USA. 2007; 104:15671–6. [PubMed: 17895376]
7. Menz RI, Walker JE, Leslie AG. Structure of bovine mitochondrial F_1-ATPase with nucleotide bound to all three catalytic sites: implications for the mechanism of rotary catalysis. Cell. 2001; 106:331–341. [PubMed: 11509182]
8. Hausrath AC, Gruber G, Matthews BW, Capaldi RA. Structural features of the γ subunit of the *Escherichia coli* F_1 ATPase revealed by a 4.4-Å resolution map obtained by x-ray crystallography. Proc Natl Acad Sci USA. 1999; 96:13697–13702. [PubMed: 10570135]

9. Stocker A, Keis S, Vonck J, Cook GM, Dimroth P. The Structural Basis for Unidirectional Rotation of Thermoalkaliphilic F_1-ATPase. Structure. 2007; 15:904–914. [PubMed: 17697996]
10. Shirakihara Y, et al. The crystal structure of the nucleotide-free $\alpha_3\beta_3$ subcomplex of F_1-ATPase from the thermophilic *Bacillus* PS3 is a symmetric trimer. Structure. 1997; 5:825–36. [PubMed: 9261073]
11. Feniouk BA, Suzuki T, Yoshida M. The role of subunit ε in the catalysis and regulation of F_OF_1-ATP synthase. Biochim Biophys Acta. 2006; 1757:326–338. [PubMed: 16701076]
12. Richter ML. Gamma-epsilon Interactions Regulate the Chloroplast ATP Synthase. Photosynth Res. 2004; 79:319–29. [PubMed: 16328798]
13. Gibbons C, Montgomery MG, Leslie AG, Walker JE. The structure of the central stalk in bovine F_1-ATPase at 2.4 Å resolution. Nat Struct Biol. 2000; 7:1055–1061. [PubMed: 11062563]
14. Campanella M, Parker N, Tan CH, Hall AM, Duchen MR. IF1: setting the pace of the F1Fo-ATP synthase. Trends Biochem Sci. 2009; 34:343–350. [PubMed: 19559621]
15. Andries K, et al. A diarylquinoline drug active on the ATP synthase of *Mycobacterium tuberculosis*. Science. 2005; 307:223–7. [PubMed: 15591164]
16. Uhlin U, Cox GB, Guss JM. Crystal structure of the ε subunit of the proton-translocating ATP synthase from *Escherichia coli*. Structure. 1997; 5:1219–1230. [PubMed: 9331422]
17. Wilkens S, Capaldi RA. Solution structure of the ε subunit of the F_1-ATPase from *Escherichia coli* and interactions of this subunit with β subunits in the complex. J Biol Chem. 1998; 273:26645–26651. [PubMed: 9756905]
18. Yagi H, et al. Structures of the thermophilic F_1-ATPase ε subunit suggesting ATP-regulated arm motion of its C-terminal domain in F_1. Proc Natl Acad Sci USA. 2007; 104:11233–11238. [PubMed: 17581881]
19. Schulenberg B, Capaldi RA. The ε subunit of the F(1)F(0) complex of Escherichia coli. Cross-linking studies show the same structure in situ as when isolated. J Biol Chem. 1999; 274:28351–28355. [PubMed: 10497194]
20. Dallmann HG, Flynn TG, Dunn SD. Determination of the 1-ethyl-3-[(3-dimethylamino)propyl]-carbodiimide-induced cross-link between the β and ε subunits of *Escherichia coli* F1-ATPase. J Biol Chem. 1992; 267:18953–18960. [PubMed: 1388160]
21. Rodgers AJ, Wilce MC. Structure of the γ-ε complex of ATP synthase. Nat Struct Biol. 2000; 7:1051–1054. [PubMed: 11062562]
22. Saita EI, et al. Activation and stiffness of the inhibited states of F_1-ATPase probed by single-molecule manipulation. J Biol Chem. 2010; 285:11441–11417.
23. Iino R, Hasegawa R, Tabata KV, Noji H. Mechanism of inhibition by C-terminal α-helices of the ε subunit of *Escherichia coli* F_OF_1-ATP synthase. J Biol Chem. 2009; 284:17457–64. [PubMed: 19411254]
24. Kabaleeswaran V, et al. Asymmetric structure of the yeast F_1 ATPase in the absence of bound nucleotides. J Biol Chem. 2009; 284:10546–51. [PubMed: 19233840]
25. Yasuda R, Noji H, Yoshida M, Kinosita K Jr, Itoh H. Resolution of distinct rotational substeps by submillisecond kinetic analysis of F_1-ATPase. Nature. 2001; 410:898–904. [PubMed: 11309608]
26. Nishizaka T, et al. Chemomechanical coupling in F_1-ATPase revealed by simultaneous observation of nucleotide kinetics and rotation. Nat Struct Mol Biol. 2004; 11:142–8. [PubMed: 14730353]
27. Kabaleeswaran V, Puri N, Walker JE, Leslie AG, Mueller DM. Novel features of the rotary catalytic mechanism revealed in the structure of yeast F_1 ATPase. EMBO J. 2006; 25:5433–42. [PubMed: 17082766]
28. Pu J, Karplus M. How subunit coupling produces the gamma-subunit rotary motion in F_1- ATPase. Proc Natl Acad Sci USA. 2008; 105:1192–7. [PubMed: 18216260]
29. Sielaff H, et al. Domain compliance and elastic power transmission in rotary F_OF_1-ATPase. Proc Natl Acad Sci USA. 2008; 105:17760–5. [PubMed: 19001275]
30. Wilkens S, Capaldi RA. Asymmetry and structural changes in ECF_1 examined by cryoelectronmicroscopy. Biol Chem Hoppe Seyler. 1994; 375:43–51. [PubMed: 8003256]

31. Zimmermann B, Diez M, Zarrabi N, Graber P, Börsch M. Movements of the ε-subunit during catalysis and activation in single membrane-bound H^+-ATP synthase. EMBO J. 2005; 24:2053–63. [PubMed: 15920483]
32. Cui Q, Li G, Ma J, Karplus M. A normal mode analysis of structural plasticity in the biomolecular motor F_1-ATPase. J Mol Biol. 2004; 340:345–72. [PubMed: 15201057]
33. Müller M, et al. Rotary F1-ATPase. Is the C-terminus of subunit γ fixed or mobile? Eur J Biochem. 2004; 271:3914–22. [PubMed: 15373837]
34. Keis S, Stocker A, Dimroth P, Cook GM. Inhibition of ATP hydrolysis by thermoalkaliphilic F_1F_O-ATP synthase is controlled by the C terminus of the ε subunit. J Bacteriol. 2006; 188:3796–804. [PubMed: 16707672]
35. Slonczewski JL, Fujisawa M, Dopson M, Krulwich TA. Cytoplasmic pH measurement and homeostasis in bacteria and archaea. Adv Microb Physiol. 2009; 55:1–79. [PubMed: 19573695]
36. Feniouk BA, Junge W. Regulation of the F0F1-ATP synthase: the conformation of subunit ε might be determined by directionality of subunit γ rotation. FEBS Lett. 2005; 579:5114–8. [PubMed: 16154570]
37. Foster JW. *Escherichia coli* acid resistance: tales of an amateur acidophile. Nature reviews. 2004; 2:898–907.
38. Mendel-Hartvig J, Capaldi RA. Nucleotide-dependent and dicyclohexylcarbodiimide-sensitive conformational changes in the ε subunit of *Escherichia coli* ATP synthase. Biochemistry. 1991; 30:10987–10991. [PubMed: 1834172]
39. Lippe G, Sorgato MC, Harris DA. The binding and release of the inhibitor protein are governed independently by ATP and membrane potential in ox-heart submitochondrial vesicles. Biochim Biophys Acta. 1988; 933:12–21. [PubMed: 2894853]
40. Fischer S, Graber P, Turina P. The activity of the ATP synthase from *Escherichia coli* is regulated by the transmembrane proton motive force. J Biol Chem. 2000; 275:30157–30162. [PubMed: 11001951]
41. Feniouk BA, Suzuki T, Yoshida M. Regulatory interplay between proton motive force, ADP, phosphate, and subunit ε in bacterial ATP synthase. J Biol Chem. 2007; 282:764–72. [PubMed: 17092944]
42. Xiong H, Zhang D, Vik SB. Subunit ε of the *Escherichia coli* ATP synthase: novel insights into structure and function by analysis of thirteen mutant forms. Biochemistry. 1998; 37:16423–16429. [PubMed: 9819235]
43. Aggeler R, Capaldi RA. Nucleotide-dependent movement of the ε subunit between α and β subunits in the *Escherichia coli* F_1F_O-type ATPase. J Biol Chem. 1996; 271:13888–13891. [PubMed: 8662953]
44. Ferrandiz MJ, de la Campa AG. The membrane-associated F_OF_1 ATPase is essential for the viability of *Streptococcus pneumoniae*. FEMS Microbiol Lett. 2002; 212:133–8. [PubMed: 12076799]
45. Rao SPS, Alonso S, Rand L, Dick T, Pethe K. The protonmotive force is required for maintaining ATP homeostasis and viability of hypoxic, nonreplicating *Mycobacterium tuberculosis*. Proc Natl Acad Sci USA. 2008; 105:11945–50. [PubMed: 18697942]
46. Jones SA, et al. Respiration of *Escherichia coli* in the mouse intestine. Infect Immun. 2007; 75:4891–9. [PubMed: 17698572]
47. Dautant A, Velours J, Giraud MF. Crystal Structure of the Mg⊗ADP-inhibited State of the Yeast F_1c_{10}-ATP Synthase. J Biol Chem. 2010; 285:29502–29510. [PubMed: 20610387]
48. Wise JG. Site-directed mutagenesis of the conserved β subunit tyrosine 331 of *Escherichia coli* ATP synthase yields catalytically active enzymes. J Biol Chem. 1990; 265:10403–10409. [PubMed: 2141332]
49. Lee RS, Pagan J, Wilke Mounts S, Senior AE. Characterization of *Escherichia coli* ATP synthase β-subunit mutations using a chromosomal deletion strain. Biochemistry. 1991; 30:6842–6847. [PubMed: 1829962]
50. Schaefer EM, Hartz D, Gold L, Simoni RD. Ribosome-binding sites and RNA-processing sites in the transcript of the *Escherichia coli unc* operon. J Bacteriol. 1989; 171:3901–8. [PubMed: 2472380]

51. Hendrickson WA, Horton JR, LeMaster DM. Selenomethionyl proteins produced for analysis by multiwavelength anomalous diffraction (MAD): a vehicle for direct determination of three-dimensional structure. EMBO J. 1990; 9:1665–72. [PubMed: 2184035]
52. Duncan TM, Bulygin VV, Zhou Y, Hutcheon ML, Cross RL. Rotation of subunits during catalysis by *Escherichia coli* F_1-ATPase. Proc Natl Acad Sci USA. 1995; 92:10964–10968. [PubMed: 7479919]
53. Otwinowski Z, Minor W. Processing of X-ray diffraction data collected in oscillation mode. Meth Enzymol. 1997; 276:307–326.
54. McCoy AJ. Solving structures of protein complexes by molecular replacement with Phaser. Acta Crystallogr D Biol Crystallogr. 2007; 63:32–41. [PubMed: 17164524]
55. Bowler MW, Montgomery MG, Leslie AG, Walker JE. How azide inhibits ATP hydrolysis by the F-ATPases. Proc Natl Acad Sci USA. 2006; 103:8646–9. [PubMed: 16728506]
56. CCP4. The CCP4 suite: programs for protein crystallography. Acta Crystallogr D Biol Crystallogr. 1994; 50:760–3. [PubMed: 15299374]
57. Emsley P, Cowtan K. Coot: model-building tools for molecular graphics. Acta Crystallogr D Biol Crystallogr. 2004; 60:2126–32. [PubMed: 15572765]
58. Adams PD, et al. PHENIX: building new software for automated crystallographic structure determination. Acta Crystallogr D Biol Crystallogr. 2002; 58:1948–54. [PubMed: 12393927]
59. Duncan TM, Zhou Y, Bulygin VV, Hutcheon ML, Cross RL. Probing interactions of the *Escherichia coli* F_OF_1 ATP synthase β and γ subunits with disulphide cross-links. Biochem Soc Trans. 1995; 23:736–741. [PubMed: 8654828]
60. Pettersen EF, et al. UCSF Chimera--a visualization system for exploratory research and analysis. J Comput Chem. 2004; 25:1605–12. [PubMed: 15264254]

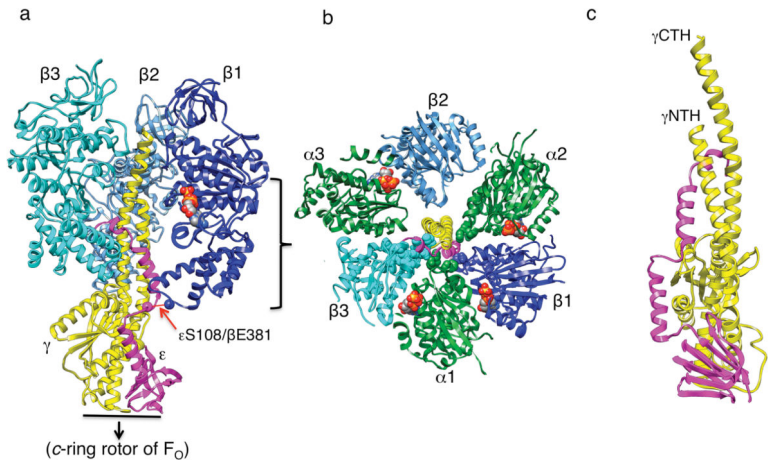

Figure 1. Overview of EF_1 structure

(**a**) Side view of EF_1 as a ribbon diagram, with α subunits omitted to reveal the portions of γ (yellow) and ε (magenta) within the central cavity. β subunits are colored in different shades of blue. Space-filling atoms are shown for ADP and SO_4 bound on β1 and for the Cα of εSer108 and β1-Glu381 (7.3 Å apart). (**b**) View from above EF_1 (53 Å cross-section, see bracket), including α subunits (green). For clarity, the only regions of γ and ε shown are γNTH, γCTH and ε109–138. Space-filling atoms are shown for all bound nucleotides (on α1, α2, α3, β1) and for residues of α and β subunits that contact ε109–138. (**c**) Rotated, magnified side view of γ and ε of EF_1.

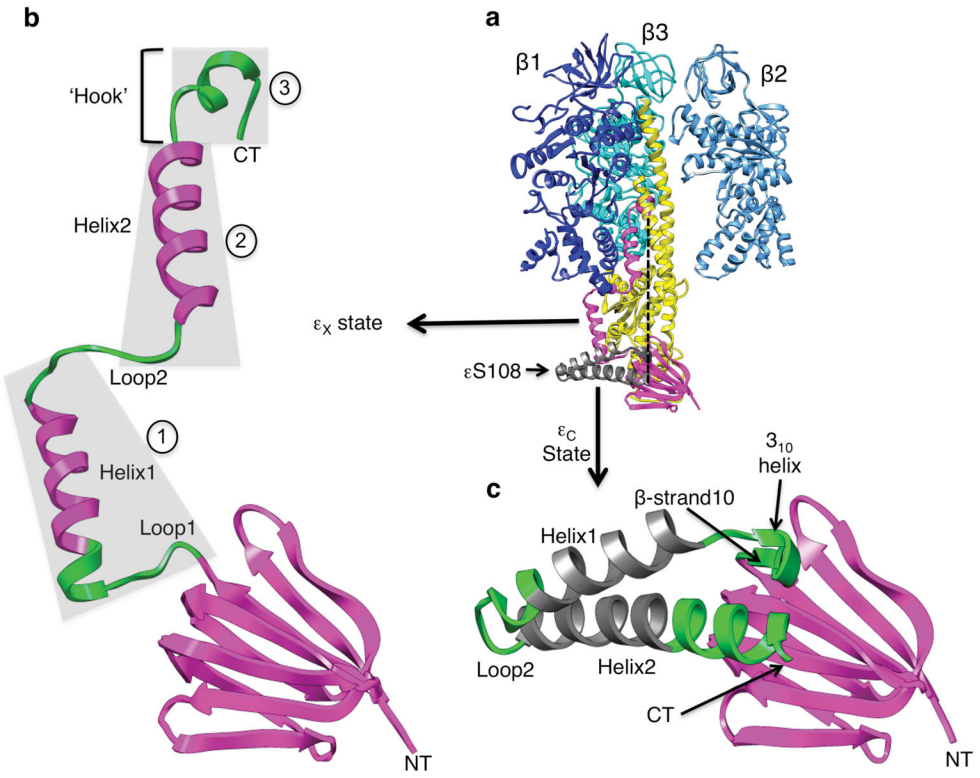

Figure 2. Comparing ε's compact and extended conformations

(**a**) Side view of EF1, omitting α subunits. Superimposed to ε's extended state in EF1 (ε_X, magenta) is the compact state of ε(ε_C) observed for isolated *E. coli* ε[16] (only εCTD is shown in gray). Between the two conformations, εNTD aligns well (RMSD ~0.67 Å, ε2–81), while there is a difference of ~73 Å in the position of ε's C-terminus (dashed line). In (**b**) and (**c**), green indicates segments of ε that differ in secondary structure between ε_X in EF_1 (**b**) and isolated ε (**c**). In (**b**) shaded areas with circled numbers identify three regions of the εCTD that contact other EF_1 subunits.

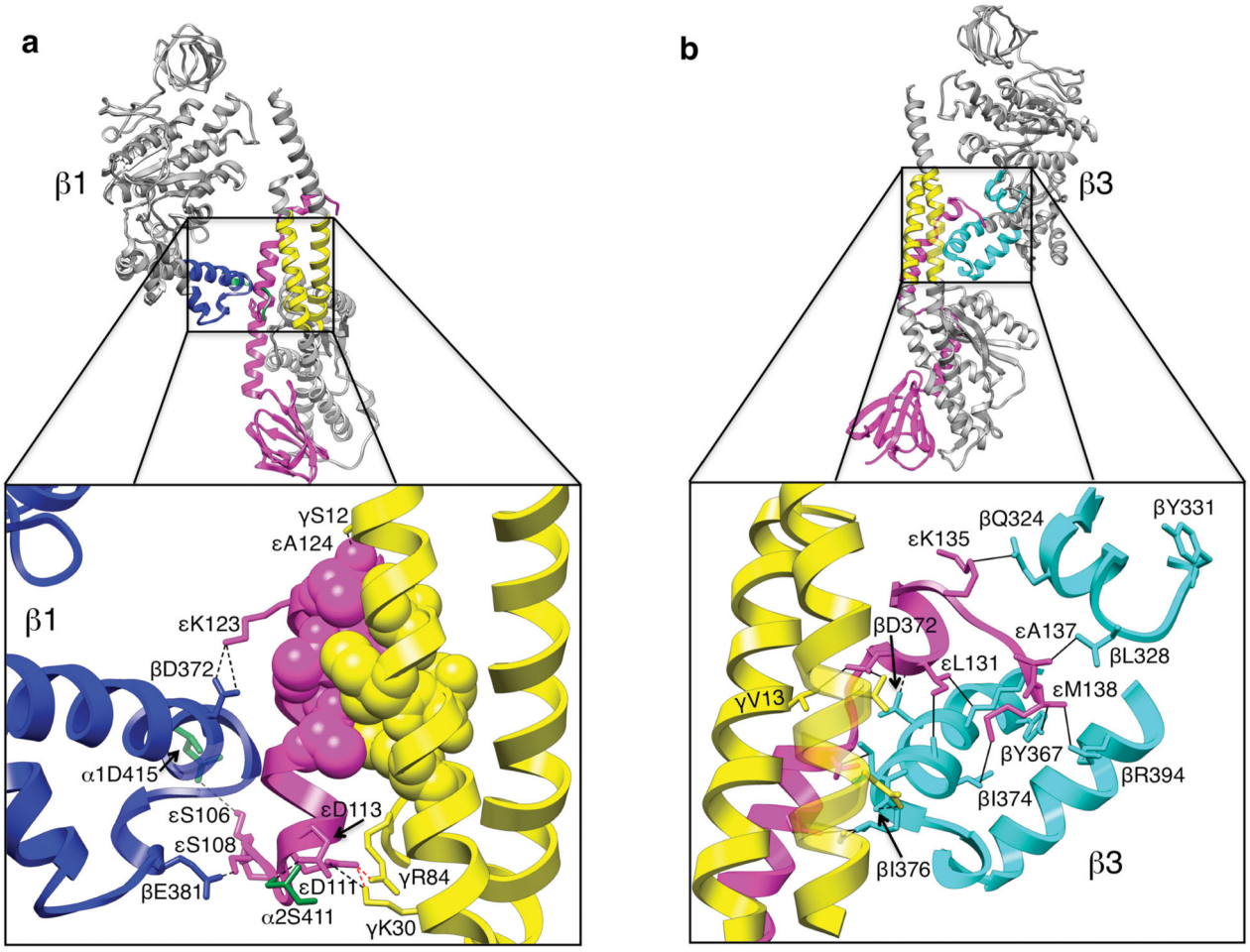

Figure 3. Interactions of εCTD within the central cavity of EF_1

Selected contact residues are shown, colored by subunit. Dashed lines represent hydrogen bonds (black) or close electrostatic contacts (red); solid black lines show van der Waals contacts. (**a**) Region-2 contacts of εCTD with γ, β1, α1, and α2. Space-filling atoms are shown for residues in the coiled-coil interface of εhelix2–γNTH. (**b**) Region-3 contacts of εCTD withβ3 and γ; βTyr331 is shown as part of the adenine-binding pocket, but no nucleotide is bound to β3 in EF_1.

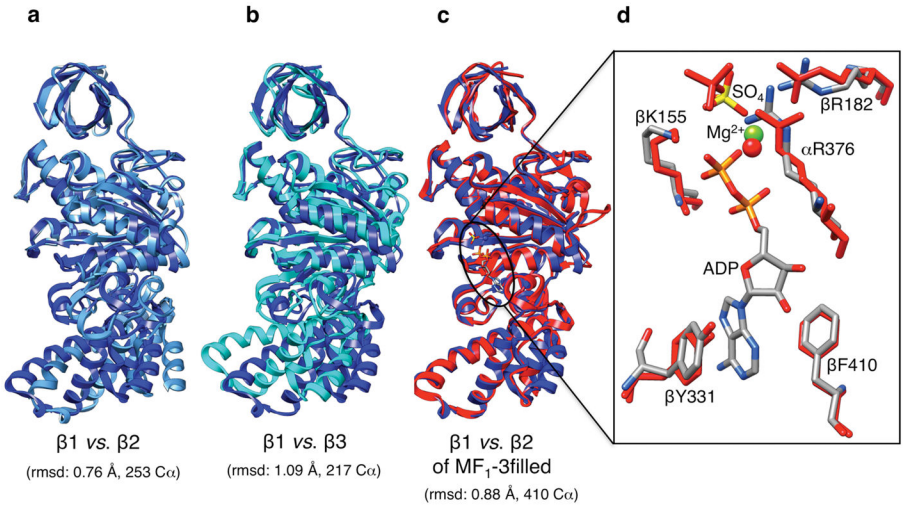

Figure 4. Distinct conformations of three β subunits in EF_1

Panels (**a**) and (**b**) show that EF1 subunit β1 (dark blue) has a conformation that is distinct from both the 'open' conformation of β2 (**a**, light blue) and the 'closed' conformation of β3 (**b**, cyan). Surveying known F_1 structures, we found that β1 of EF_1 superimposes best with the 'half-closed' conformation of β2 in the bovine MF_1 structure that has nucleotide bound at all 3 catalytic sites (MF_1-3filled)[7] (panel **c**, red). For the superimposition of panel (**c**), panel (**d**) focuses on details at the catalytic nucleotide-binding site. For β1 of EF_1, (**b**) shows atom-colored sticks for bound ligands ADP and SO_4^{2-} (Mg^{2+} = green sphere) and for five key residues (numbered); the corresponding residues, SO_4^{2-} and Mg^{2+} are shown in red for β2 of MF_1-3filled (bound ADP is oriented similar to ADP on β1 of EF_1 and is omitted for clarity).

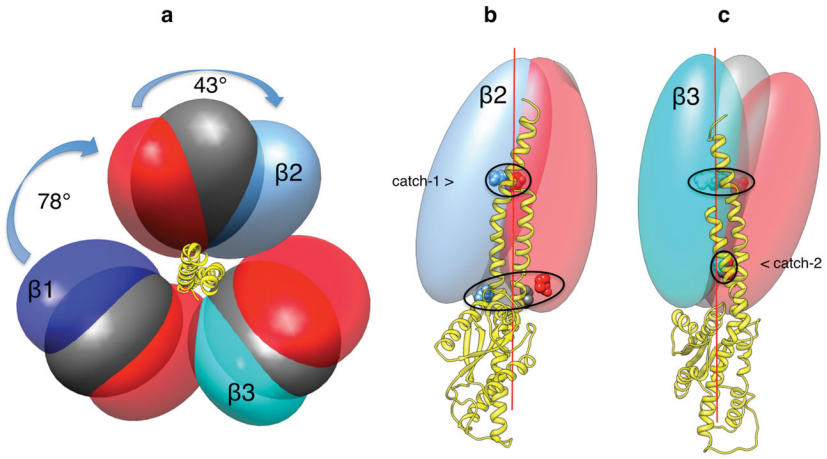

Figure 5. Insights for rotary mechanics of ATP synthase

(**a**) View from below F1 with a ribbon diagram of the γNTH–γCTH coiled-coil (EF_1) and mass-weighted ellipsoids for β subunits of three F_1 structures superimposed by γ's structural core (Supplementary Fig. 5). Specific βs are labelled for EF_1 (shades of blue), and corresponding βs are shown for yF_1II^{27} (gray) and bovine MF_1(3-filled) (red). Arrows indicate the rotation needed (in hydrolysis direction) to superimpose β1 of EF_1 with β2 of MF_1(3-filled) (78°) or to superimpose β2 of MF_1(3-filled) with β2 of EF_1 (43°). (**b**) and (**c**) side views of *E. coli* γ with the ellipsoids of either β2 (**b**) or β3 (**c**) for the three γ-aligned F_1 structures. For each β ellipsoid in (**b**) and (**c**), two residues are shown: βAsp305 (in 'catch 1', β2–γ) and βIle376 (in 'catch 2', β3–γ). The red line (**a,c**) is the axis for the 78° rotation noted in (**a**).

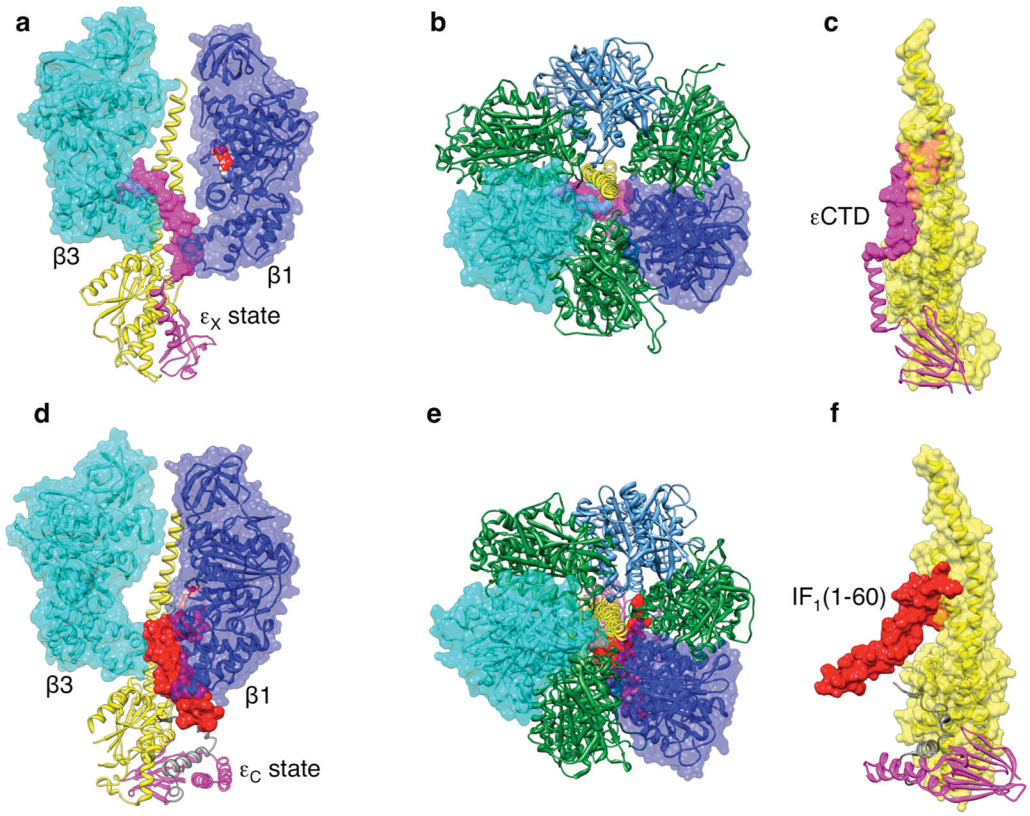

Figure 6. Comparing interactions with F_1 for *E. coli* εCTD and the mitochondrial inhibitor IF_1

Side and top views are shown for EF_1 (**a,b**) and MF_1+$IF_1(1–60)^6$ (**d,e**). The same viewpoints of EF_1 and MF_1+ $IF_1(1–60)$ are aligned by the γ-core. Side views show only β1, β3, γ and ε (or its magenta-colored homolog, $δ_M$), plus unique mitochondrial chains $ε_M$ (gray) and IF_1 (red) (**d,e**). Solvent-excluded surfaces are shown for β1 and β3 (ADP shown if present), and ε106–138 (**a**) or IF_1 (**d**). In (**c**) and (**f**) (view rotated 120° from (**a/d**), α and β subunits are omitted and a transparent, solvent-excluded surface is added for γ in EF_1 (**c**) and in MF_1+$IF_1(1–60)$ (**f**).

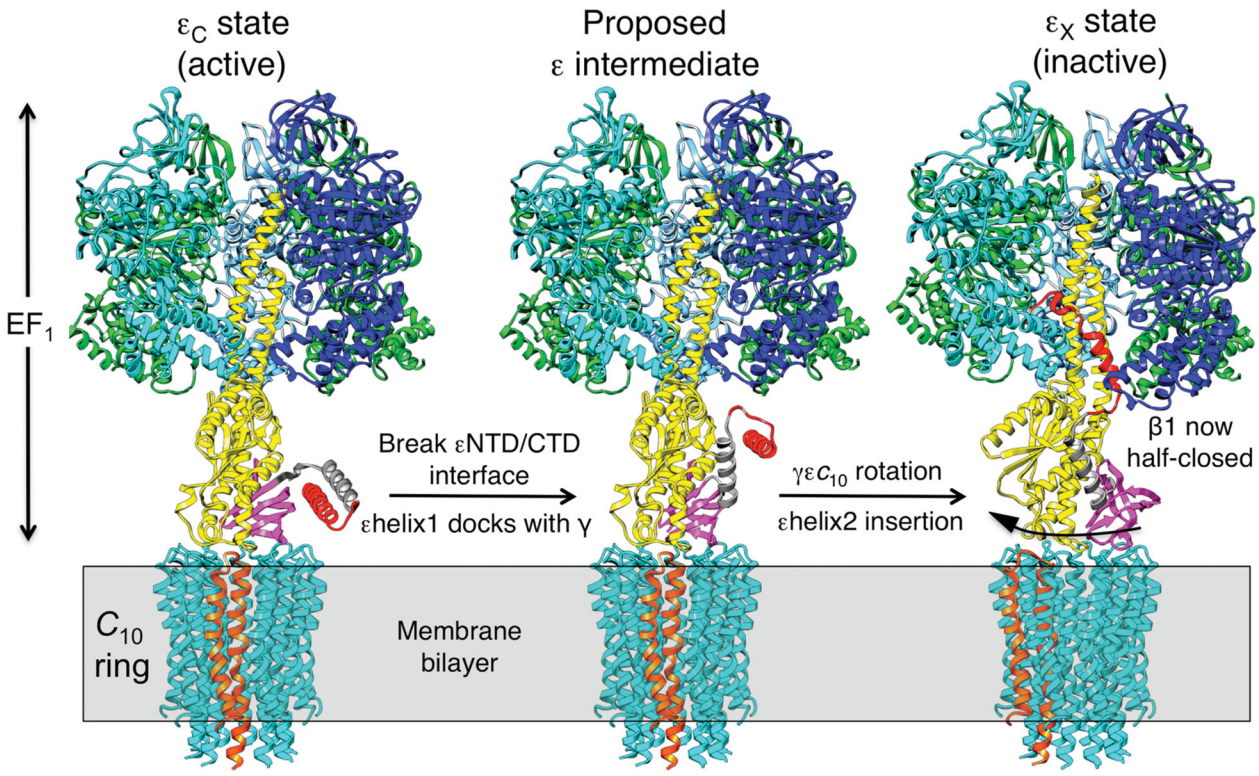

Figure 7. Model for transition between ε_C and ε_X states in EF_1

Models of EF1 are docked with the $\boldsymbol{c}_{10}$–ring of F_O from a yeast MF_1–$\boldsymbol{c}_{10}$ structure[47] (EF_1 and MF_1 superimposed by γ-core). The membrane is depicted by the gray region. Not shown is the $\boldsymbol{ab}_2\delta$ stator assembly, which has not yet been resolved. In each EF_1 model, regions of ε are colored magenta (εNTD), gray (ε82–105) or red (ε106–138), and subunit α1 is omitted to view the central cavity. The determined structure of EF_1 (right) has the rotor assembly ($\gamma\varepsilon\boldsymbol{c}_{10}$) rotated ~40° (in hydrolysis direction) relative to the other two models. A specific ***c*** subunit (orange) provides a visual reference for the rotation.

Table 1

Data collection and refinement statistics

	EF_1-δ	SeMet-EF_1-δ
Data collection		
Space group	C2	C2
Cell dimensions		
a, *b*, *c* (Å)	435.97, 183.00, 225.39	432.39, 181.71, 224.34
α, *β*, *γ* (°)	90.00, 108.99, 90.00	90.00, 109.44, 90.00
Resolution (Å)	30–3.26 (3.34–3.26)*	50–5.00 (5.18–5.00)*
R_{sym}	9.2(62.7)	17.4(58.5)
$I/\sigma I$	15.4(1.5)	8.9(2.0)
Completeness (%)	98.5(91.7)	97.8(90.2)
Redundancy	2.5(2.1)	3.4(2.5)
Refinement		
Resolution (Å)	15–3.26	
No. reflections	252,275	
R_{work}/R_{free}	24.31/26.48	
No. atoms		
Protein	99,621	
Ligand/ion	16/32	
Water	66	
B-factors (Å^2)**		
Protein	99	
Ligand/ion	91/93	
Water	53	
R.m.s. deviations		
Bond lengths (Å)	0.004	
Bond angles (°)	0.821	

* Values in parentheses are for highest-resolution shell.

** Average B-factor values refer to EF1-1.